Localized Rapid Heating by Low-Power Solid-State Microwave Drill

Yehuda Meir, *Student Member, IEEE*, and Eli Jerby, *Member, IEEE*

***Abstract*—This paper presents a theoretical and experimental study of a locally induced microwave-heating effect implemented by a low-power transistor-based microwave drill. A coupled thermal–electromagnetic model shows that the thermal-runaway instability can be excited also by relatively low microwave power, in the range ∼ 10-100 W, hence by solid-state sources rather than magnetrons. Local melting then occurs in a millimeter scale within seconds in various materials, such as glass, ceramics, basalts, and plastics. The experimental device employs an LDMOS transistor in an oscillator scheme, feeding a miniature microwave-drill applicator. The experimental results verify the rapid heating effect, similarly to the theoretical model. These findings may lead to various material-processing applications of local microwave heating implemented by solid-state devices, including local melting (for surface treatments, chemical reactions, joining, etc.), delicate drilling (e.g., of bones in orthopedic operations), local evaporation, ignition, and plasma ejection (e.g., in microwave-induced breakdown spectroscopy (MIBS) for material identification).**

***Index Terms*—Hotspots, laterally diffused metal–oxide semiconductor field-effect tranLDMOS-FET, microwave drills, microwave heating, thermal-runaway instabilities.**

I. Introduction

THE self-focused heating effect caused by the microwave drill [1], [2] is attributed to the intentional thermal-runaway instability induced in the processed material. This effect occurs in materials in which the dielectric and thermal properties depend on the temperature [3]; thus, the hotspot is evolved rapidly up to the melting point. Further microwave irradiation may cause also evaporation and even plasma ejection from the hotspot [4]. The microwave-drill effect was demonstrated in various materials, including concrete, glass, ceramics, basalts, silicon, and bones [5]–[12]. Unlike the remote laser-based drill, the heat-affected zone (HAZ) of the near-field microwave drill is smaller than the electromagnetic (EM) wave wavelength λ (e.g., for $\lambda \sim 12$ cm at 2.45 GHz, the molten region is typically $< 1\text{-cm}^{\emptyset}$).

Similar near-field microwave-heating effects induced by open-end applicators were studied for various applications, including silicon heating [13] and doping [14], electrochemical processes in liquids [15]–[18], interstitial treatment [19], [20], and tissue heating [21] and ablation [22] for cancer treatment.

The microwave-drill capabilities presented in the literature were demonstrated mostly by magnetron tubes of 600–900 W, as used in domestic microwave ovens. These require 4-kV power supplies, waveguide sections, and impedance-matching elements, which might be too cumbersome for portable machines or for delicate operations. Hence, using compact solid-state microwave sources, instead of magnetrons, in local-heating systems could reduce their size, weight, and operating voltage and improve their spectral characteristics, tunability, and controllability. A similar transition from vacuum to solid-state electronics was considered for volumetric (nonlocal) microwave heating [23], [24], yet most of the microwave-heating systems employ magnetrons.

The emerging cellular network technology and the growing need for base-station transmitters advanced the development of $>$ 100-W RF transistors [25]. Consequently, gallium–nitride (GaN) [26], silicon–carbide (SiC) [27], and silicon-based laterally diffused metal–oxide semiconductor (LDMOS) [28] technologies became more relevant to microwave-heating applications as well. The solid-state microwave-drill feasibility for delicate operations has been introduced in several conferences [29], [30].

This paper comprehensively presents the discovery that, under proper conditions, the microwave-drill effect [1]–[3] may occur in much lower power than published before. The reduction reported here, from $\sim$ 600 W to the order of 10 W, is enabled by designing the miniaturized device in a form that concentrates the power density required for softening the drilled material in a smaller area. The consequent power reduction enables the microwave-drill advancement from magnetron- to transistor-based systems in various applications. This transition from vacuum to solid-state electronics (less common in microwave heating than other fields) could be revolutionary for the microwave-drill compactness, effectiveness, simplicity, and cost, and it opens also new scientific possibilities (e.g., miniature devices incorporated within synchrotrons in order to explore *in situ* localized microwave-heating effects [4]). The new solid-state implementation removes obstacles that impeded the proliferation of the microwave-drill technology in the former magnetron-based schemes, particularly for delicate applications (such as bone drilling in orthopedic operations [11]). To the best of the authors' knowledge, this paper presents for the first time a methodological microwave-drill design and a comparison of the microwave-drill theory to experiments. The theoretical analysis confirms the microwave-drill feasibility in the new 10–100-W range, in agreement with experiments. A simple heuristic *drillability* factor is introduced and compared

Manuscript received February 13, 2012; revised March 15, 2012; accepted March 19, 2012. Date of publication June 11, 2012; date of current version July 30, 2012. This work was supported by the Israeli Science Foundation under Grant 1270/04 and Grant 1639/11.

The authors are with the Faculty of Engineering, Tel-Aviv University, Ramat Aviv 69978, Israel (e-mail: jerby@eng.tau.ac.il).

Color versions of one or more of the figures in this paper are available online at http://ieeexplore.ieee.org.

Digital Object Identifier 10.1109/TMTT.2012.2198233

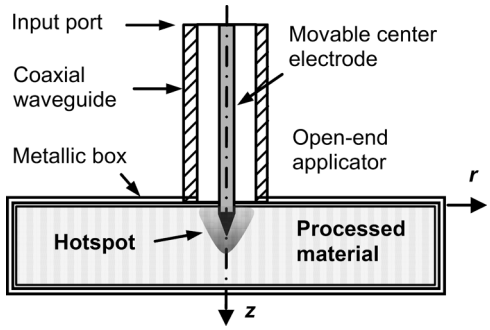

Fig. 1. Microwave-drill scheme consisting of a coaxial open-end applicator with a movable center electrode which penetrates into the softened hotspot.

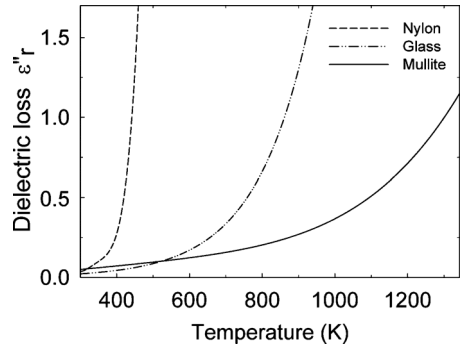

Fig. 2. Temperature dependence of the dielectric-loss factor in Nylon, glass, and mullite [32]–[34].

with theory. New potential nondrilling applications of the transistor-based microwave drill, as a localized heater in free space, are proposed and demonstrated as well.

II. Theoretical Model

The theoretical model [3] is presented briefly for the sake of self-consistency in order to validate the feasibility of the new 10–100-W microwave-drill regime (note that the model was introduced before for 800-W systems, whereas performance degradation was indicated at 600 W due to lack of power). The new theoretical results are compared also with the *drillability* factor and with experimental results (presented in Sections III and IV).

The locally induced thermal-runaway instability is simulated by a coupled EM-thermal model that takes into account the temperature dependence of the material's properties and the varying geometry [3]. The model combines the EM-wave equation and the heat equation in an inhomogeneous medium. As illustrated in Fig. 1, the processed material situated in a metallic box is irradiated locally via a coaxial applicator.

The coupled EM-wave and heat equations are presented in a two-time-scale approach by

$$\nabla \times \left(\mu_r^{-1} \nabla \times \tilde{\mathbf{E}}\right) - \left[\varepsilon_r' - j\left(\varepsilon_r'' + \frac{\sigma}{\omega \varepsilon_0}\right)\right] k_0^2 \tilde{\mathbf{E}} = 0 \quad (1)$$

$$\rho C_p \frac{\partial T}{\partial t} - \nabla \cdot (k_{th} \nabla T) = Q \quad (2)$$

where $\tilde{\mathbf{E}}$ is the electric vector component of the EM wave in the frequency domain, and ω and k_0 are its angular-frequency and free-space wave-number, respectively. The processed material is represented by μ_r, which is the relative magnetic permeability, $\varepsilon_r = \varepsilon_r' - j\varepsilon_r''$, the complex relative dielectric permittivity, and σ, which is the electric conductivity. In the heat equation (2), ρ is the local density of the processed material, C_p and k_{th} are its heat capacity and thermal conductivity, respectively, and T is the slowly varying temperature. The material parameters ε_r, σ, ρ, C_p, and $k_{\rm th}$ are considered as having known temperature dependencies.

The distinction between the typical time scales of the EM wave propagation and the slower thermal evolution ($\sim$ 1 ns versus $>$ 1 ms, respectively) allows the *two-time scale* approximation. Its validity is verified by the heuristic condition $\rho C_p d_{hs}^2 / k_{th} \gg \tau$, where d_{hs} is the hotspot width and $\tau = 2\pi/\omega$ is the wave period. The EM bandwidth is sufficiently narrow to neglect the permittivity's frequency variation, hence the wave equation (1) is solved in the frequency domain while the heat equation (2) is computed in the slowly varying time domain. Equations (1) and (2) are coupled together by the local EM heating source

$$Q = \omega \varepsilon_0 \varepsilon_r''(T) \frac{|\tilde{\mathbf{E}}|^2}{2} \quad (3)$$

and by the consequent variations of the material parameters ε_r, σ, ρC_p, and $k_{\rm th}$, with temperature [31]. As the temperature rises, the spatial variations in ε_r and σ modify the microwave radiation pattern, hence enabling the self-focusing effect.

The dielectric loss-factor $\varepsilon_r''(T)$ in materials such as Nylon (Ertalon-6), mullite, and soda-lime glass [32]–[34] tends to increase as the temperature rises, as shown in Fig. 2. Hence, a larger amount of thermal energy is dissipated locally, and, consequently, the temperature's rising rate increases further. The hotspot is created by thermal-runaway instability which is ceased by a phase transition, namely by melting, evaporation, or breakdown of the material in the hotspot, forming liquid, gas, or plasma, respectively. The thermal-runaway instability [35] is known in volumetric microwave applicators as a cause of accidental damages to the processed material, thus it needs to be stabilized [36]. Here, this instability is initiated intentionally for the sake of local processing, hence it is defined here as an *induced thermal-runaway instability*. In order to achieve local melting and drilling by virtue of the induced thermal runaway effect, the energy concentrated by the self-focusing effect in the hotspot should be as dense as possible. However, in order to study the feasibility range of the transistor-based microwave-drill applicator, the power should be relatively low ($<$ 100 W). Hence, the purpose of this study is to find the minimal input power that can still initiate the hotspot and enable the microwave drilling.

The coupled EM-thermal equation [(1)–(3)] are solved here by COMSOL Multiphysics using a finite-difference time-domain (FDTD) algorithm for the heat equation and a finite-element frequency-domain solver for the EM equations. The solution of this nonlinear system is simplified by the two-time scale approximation and by the cylindrical symmetry of the device. In the numerical model, the outer box (Fig. 1) is a perfect electric conductor (PEC). The boundary conditions for the heat equation

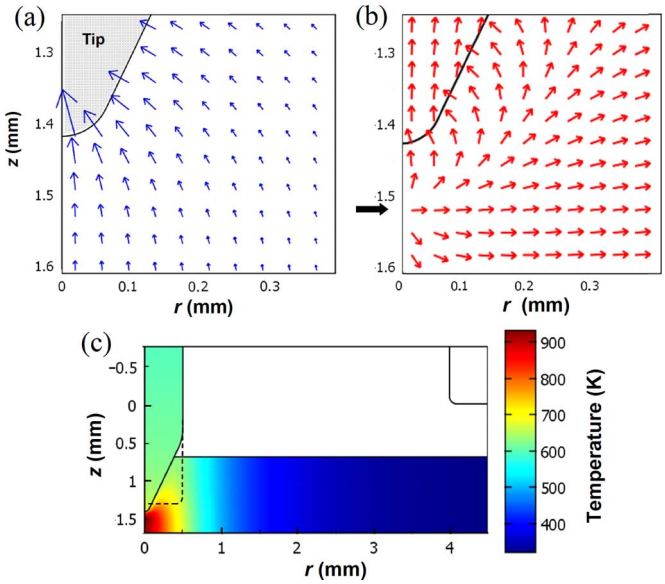

Fig. 3. Numerical simulation of the confined hotspot formed in a 1-mm-thick soda-lime glass plate irradiated by 80-W microwave power at 2.1 GHz. The results are shown after 17 s, when the glass reaches its softening temperature. (a) Electric-field vectorial distribution exceeding 3.5×10^6 V/m. (b) Normalized heat flux in the vicinity of the drill bit with a virtual origin marked by a black arrow. (c) Temperature distribution exceeding 930 K with the sharpened tip (the dashed line shows a nonoptimized configuration which fails to induce rapid local heating).

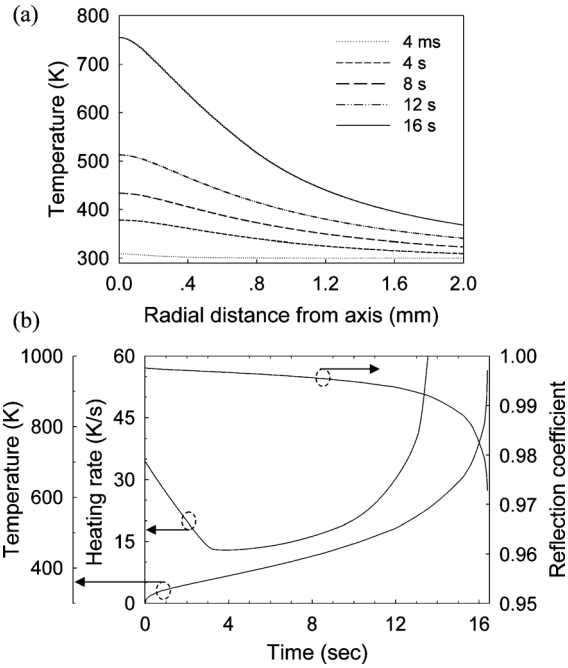

Fig. 4. Simulation results for a 1-mm-thick soda-lime glass plate heated locally by 80 W at 2.1 GHz (a) Temperature profile evolution. (b) Reflection coefficient, peak temperature, and heating rate evolved.

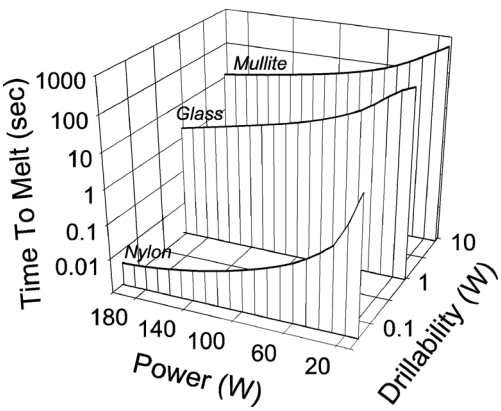

Fig. 5. TTM computed for Ertalon-6, soda-lime glass, and mullite at different microwave power levels and their corresponding drillability factors [see (4)].

assume heat convection to the surrounding air and a negligible blackbody radiation from the surface.

Fig. 3(a)–(c) shows simulation results of a 1-mm-thick soda-lime glass plate heated locally by 80 W at 2.1 GHz. The glass softening temperature ($\sim$ 930 K) is reached near the electrode in 17 s. The electric field profile inside the glass [the proportional vector plot in Fig. 3(a)] reveals the dominance of the axial electric field component (exceeding 3.5×10^6 V/m) in front of the electrode tip. The normalized heat flux vectors [Fig. 3(b)] reveal the heat origin in a focal point, $\sim$ 0.1 mm underneath the tip within the glass substrate; hence the heat is induced locally by the microwave radiation guided by the tip. The temperature distribution [Fig. 3(c)] shows the hotspot confinement in a 1-mm$^{\emptyset}$ region, exceeding 930 K with the sharpened tip. The optimized electrode shape enables the material softening in the given area and power. For the sake of comparison, the dashed line in Fig. 3(c) shows another (nonoptimized) tip configuration that fails to induce rapid local heating in the same operating conditions. With respect to previous studies [1]–[3], the sharpened tip and its narrower diameter provide the power concentration required for the intentional thermal-runaway effect in the lower power.

The temperature profile evolution during the localized microwave heating in the conditions of Fig. 3(a)–(c) is shown in Fig. 4(a). The hotspot diameter ($\sim$ 1-2 mm$^{\emptyset}$) is measured at different times by the full-width half-maximum (FWHM) values of the Gaussian-like curves. Fig. 4(b) shows the simulation results for the evolution of the peak temperature, the microwave reflection coefficient, and the heating rate, for 80 W. A 25% increase from 80 to 100 W shortens the time-to-melt (TTM) by 37%. The distinction between the initial inflation of the hotspot region and its final shrinkage coincides with the heating rate changes from descending to ascending after $\sim$ 3 s. The drop in the reflection coefficient and the rapid rise of the peak temperature indicate the hotspot formation [compared below with the experimental results shown in Fig. 9(a)]. On the contrary, the heating rates obtained by nonoptimized electrode geometries are much slower. For example, the flat tip illustrated by the dashed line in Fig. 3(c) needs more than 80 s to reach thermal runaway [compared with 17 s for the optimized tip in Fig. 4(b)].

A simplified heuristic condition for the hotspot initiation is proposed as $W > D$ [30], where W is the net microwave power absorbed in the hotspot region and D is given by

$$D = 2.5 k_{\mathrm{th}} \frac{d_{hs} \Delta T_m}{\Delta \varepsilon''_r}. \tag{4}$$

In (4), ΔT_m is the difference between the melting and room temperatures, and $\Delta \varepsilon''_r$ is the corresponding difference in the rela-

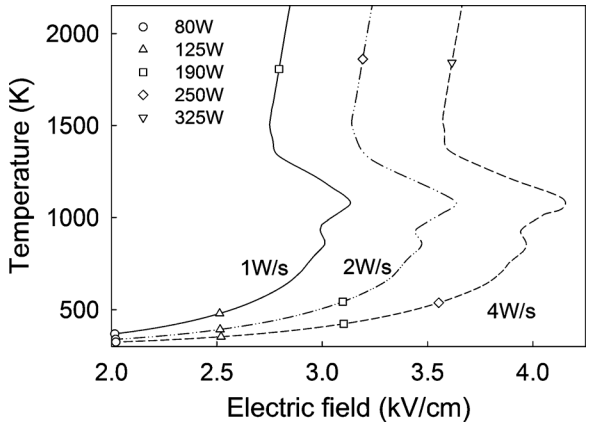

Fig. 6. Calculated S-shaped curves for localized heating of mullite at different rates of input-power increase. The discrete power values indicate the microwave power involved on each curve.

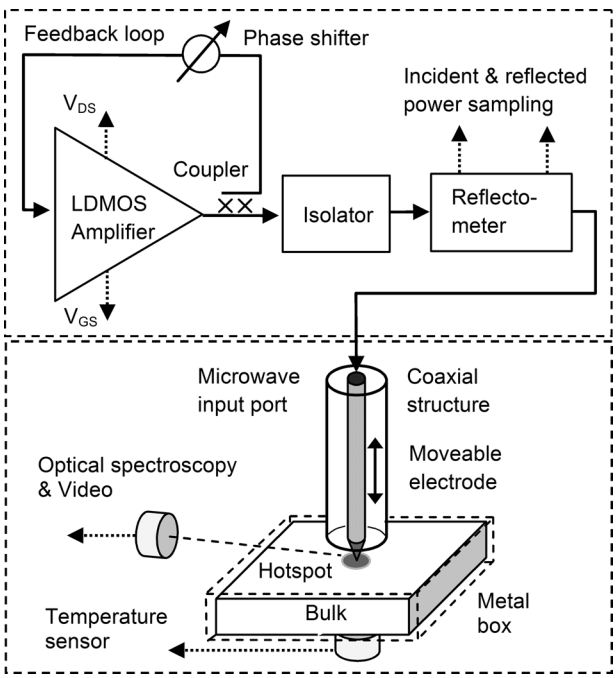

Fig. 7. Experimental scheme of the transistor-based microwave-drill localized heater, consisting of an LDMOS amplifier with a positive feedback loop feeding a coaxial open-end applicator with a movable center electrode. The dotted lines denote signals sampled by a LabVIEW interface.

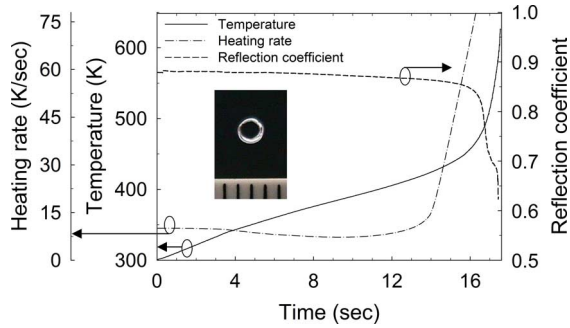

Fig. 8. Experimental demonstration of the induced thermal runaway effect, hotspot formation, melting, and drilling in glass by 80-W microwave power applied locally to a 1-mm glass plate. The graph shows the temporal evolution of the temperature, the heating rate, and the microwave reflection coefficient. The inset shows a typical $\sim$ 1-mm$^{\emptyset}$ hole made under these conditions.

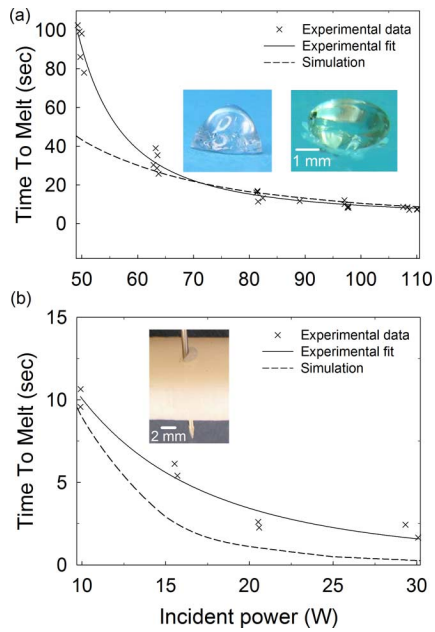

Fig. 9. Measured TTM values and their exponential curve fit ($a\exp[b/(x+c)]$) compared with theoretical results for 1-mm-thick plates. (a) Soda-lime glass. The insets show the hole made (right) and the removed glass chunk (left). (b) An Ertalon-6 plate. The inset shows the electrode inserted into the plate.

tive dielectric-loss factor. The parameter D provides a rough estimate for the net minimal microwave power needed to initiate the induced thermal-runaway process, hence it is regarded as a *drillability factor* in the context of the microwave-drill operation. The condition $W > D$ can be satisfied in power levels of $\sim$ 10-100 W for a variety of practical materials, except transparent dielectrics such as pure alumina and sapphire.

For the sake of comparison, the drilling operation was simulated numerically in 1-mm-thick slabs of mullite, glass, and Nylon. These materials differ significantly by their properties, hence the drillability factors characterizing them are 8.58, 0.92, and 0.05 W, respectively. Fig. 5 shows the TTM resulted from the simulation with respect to the microwave power applied. In the power level of $\sim$ 100 W, the TTM is in the order of $\sim$ 0.1 s in Nylon, $\sim$ 10 s in glass, and $\sim$ 1 min in mullite, in accordance with their drillability factor values.

The thermal-runaway instability in *volumetric* microwave heating is characterized by a bi-stable S-shaped curve of the temperature versus the electric field [37]. The temperature rise on the lower branch till it reaches the meta-stable region in which the thermal-runaway instability occurs hence it jumps to the steeper branch. A similar behavior is identified here in the *locally induced* thermal-runaway effect, as demonstrated in Fig. 6 for localized heating of mullite at different rates below the melting temperature.

Besides the dielectric and thermal parameters included in the model, the microwave-drilling feasibility is affected also by the material's thermal expansion and hardness properties. Hence, materials like sapphire and pure alumina are less adequate for

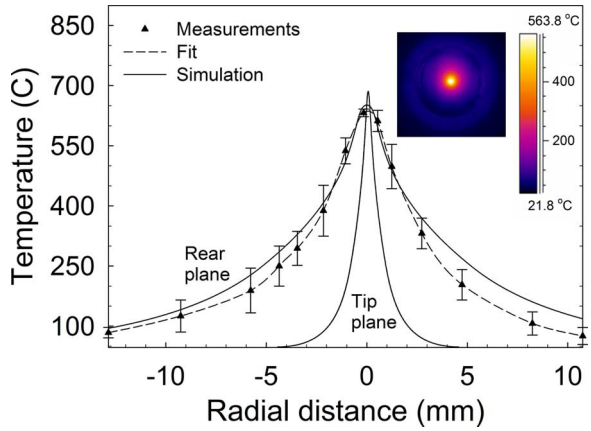

Fig. 10. Temperature profile detected on the rear surface of a 1-mm glass plate by a thermal camera (FLIR E40) and its fit. The solid curves show the numerical simulation result for the temperature profiles at the tip ($z = 0.5$ mm) and rear planes. The inset shows the FLIR image.

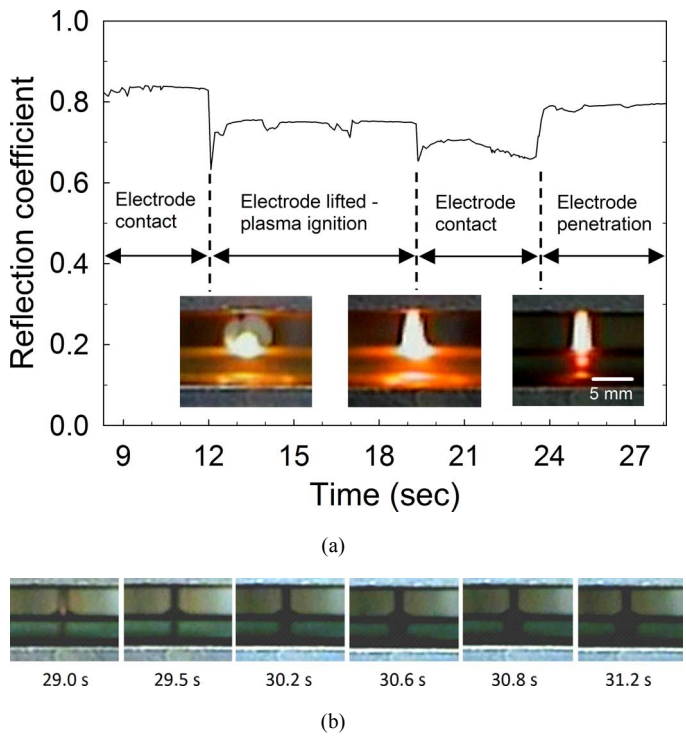

(a)

(b)

Fig. 11. (a) Microwave drilling process in soda-lime glass enhanced by plasma ejection. The various stages are seen by the reflection coefficient variations, and visually by the side-view images in the insets. (b) Side view of the devitrification process and porosity formation in hot glass cooling down after the microwave is turned off. The dark region inside the glass shows the porosity expansion around the electrode.

microwave drilling *per se*, though they can be treated by plasma excitation as a pre-heating stage [4], [7] [e.g., as in Fig. 11(a)].

III. Experimental Setup

The experimental setup is illustrated in Fig. 7. It consists of a coaxial open-end applicator with a 1-mm$^{\emptyset}$ movable electrode, fed by a solid-state amplifier with a positive feedback. The LDMOS-FET amplifier (Freescale MRF 6S21140 evaluation board) is tuned by the feedback loop to oscillate at 2.1 GHz. It can generate up to 140-W CW power, controlled by the $V_{\rm GS}$ and $V_{\rm DS}$ voltages. The transistor is protected from the microwave reflections by an isolator. The incident and reflected waves are detected by a reflectometer which consists of a directional coupler and Schottky diodes.

The center electrode of the coaxial open-end applicator is moveable. Thus, its tip can be penetrated into the softened hotspot evolved in the substrate material. An infrared temperature sensor (Raytek CI3) measures the temperature at the bottom surface of the heated material during the process. A video camera captures images of the local heating process via a side aperture. The operating signals (marked by doted arrows in Fig. 7) are sampled by a LabVIEW interface card in a 100-sample/s rate. The data and video files are logged on a PC for further analyses.

IV. Experimental Results

The feasibility of the localized microwave-heating effect is demonstrated here experimentally in the range 10–100 W using the solid-state apparatus shown in Fig. 7. Fig. 8 shows measurements of the temperature evolution and the microwave reflection during the local heating of a 1-mm-thick soda-lime glass plate by 80-W incident power. The heating rate reveals the turning point of the induced thermal runaway process ($t \sim 14$ s) accompanied by an abrupt decrease in the microwave reflection due to the better absorption of the microwave energy by the hotter material. These resemble the theoretical results shown in Fig. 4(b), whereas the differences stem from practical reasons (e.g., the measured reflection includes the losses of the coaxial line between the oscillator and the applicator, and similarly the temperature measured at the bottom surface of the glass plate is delayed due to heat diffusion).

The TTM parameter provides a unified measure for the induced thermal-runaway process in different materials as demonstrated theoretically in Fig. 5. Fig. 9(a) shows experimental results of 25 TTM measurements obtained in different microwave power levels in 1-mm-thick glass plates, as in Fig. 8. The incident power in the range 50–110 W was held fixed in each run. The TTM measurements with respect to power were fitted and compared with the theoretical results. The agreement between the experiments and theory is satisfying in the range 60–110 W with a $< 20\%$ difference. The deviation at 50 W is attributed to the parametric sensitivity in this limit, which is the minimal power level in which the thermal-runaway effect could be initiated in these conditions.

Fig. 9(b) shows similar TTM experiments performed in Ertalon-6 slabs, which result in a similar descending dependence on the incident power. The experimental result agrees reasonably with the theory around $\sim$ 10 W, in which the TTM is ~ 10 s, but deviates at higher power levels (note that the shorter TTM are less accurately measured). The tendencies observed experimentally in Fig. 9(a) and (b) resemble the theoretical results presented in Fig. 5.

The molten hotspot is observed in a glass plate also via its rear surface. The temperature profile evolved is detected there by a thermal camera (FLIR E40) positioned as the temperature sensor in Fig. 7. The thermal image and the temperature profile observed at the melting point are shown in Fig. 10. The theoretically computed temperature profiles at the tip and rear

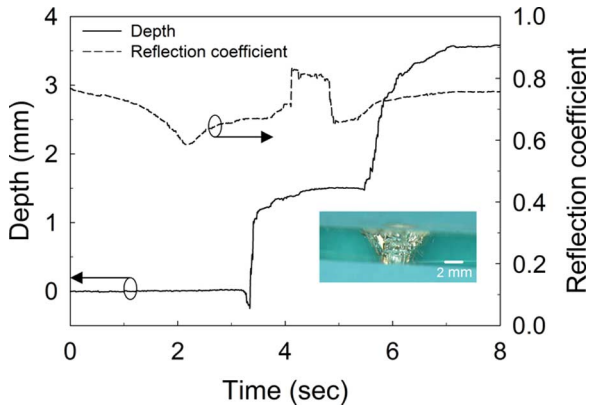

Fig. 12. Spontaneously stepwise microwave drilling in a 4-mm-thick glass plate. Each step is initiated by a hotspot which enables the electrode penetration to a ∼ 2-mm depth. The progress is then delayed until another deeper hotspot is evolved and enables a further penetration. The inset shows a crosscut in the glass plate.

planes are shown for comparison. The difference between the curves demonstrates the thermal diffusion through the 1-mm-thick glass plate. The hotspot confinement effect is clearly seen in Fig. 10.

The microwave local heating effect, and in particular the drilling process, can be enhanced by a slight plasma ejection from the heated surface toward the electrode. After the initial stage of local microwave heating, the electrode is lifted for a few seconds in order to generate plasma [4], [7] which assists the local preheating and alleviates the next stage of the microwave-drilling process. The additional plasma stage is shown in Fig. 11(a) for microwave drilling of a 4-mm-thick glass plate by a graphite electrode at 80-W incident power. The various stages of the electrode manipulation and plasma excitation are seen by the reflected microwave power.

After the microwave is turned off in Fig. 11(a), the molten glass cools down with the electrode inserted in it, as shown in Fig. 11(b). The region around the electrode begins to solidify into a porous glass, expanding from the drill bit outwards. The devitrification process is clearly seen by the growing dark region around the drill bit within the glass in a ∼ 2-s period.

A stepwise microwave drilling process occurs in deeper insertions. Fig. 12 shows the effect in a 4-mm-thick glass plate subjected to 70-W input power. The stepwise progress under a modest mechanical force implies that two successive hotspots are formed during the process in two different depths, as indicated by the microwave reflection drops. The first hotspot enables the initial penetration, which could be continued further only after the second hotspot has formed underneath. The stepwise microwave drilling, with two steps of ∼ 2-mm each, provides also a rough measure of the hotspot depth, which coincides with the theoretical results.

The porous region of ∼ 3-mm$^{\emptyset}$ presented in Fig. 11(b) can be removed by a slight mechanical grinding in order to enlarge the hole. Fig. 13(a) shows an example of such porosity in a 4-mm-thick glass plate processed locally as in the first step in Fig. 12. Hence, the mechanically assisted microwave-drilling method consists of repeating stages of applying the microwaves again on the same spot, cooling it down and then removing the

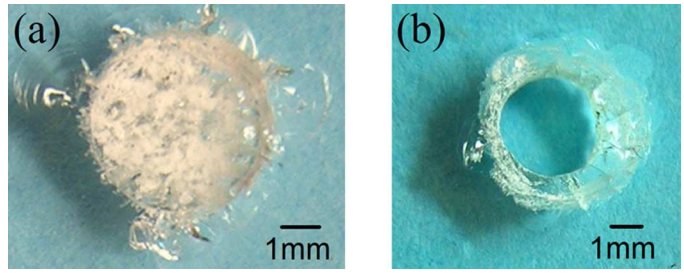

Fig. 13. Mechanically assisted microwave drilling in glass. (a) Porous region is formed by the localized microwave impact. (b) Porous glass is removed by a slight mechanical grinding in order to deepen the hole.

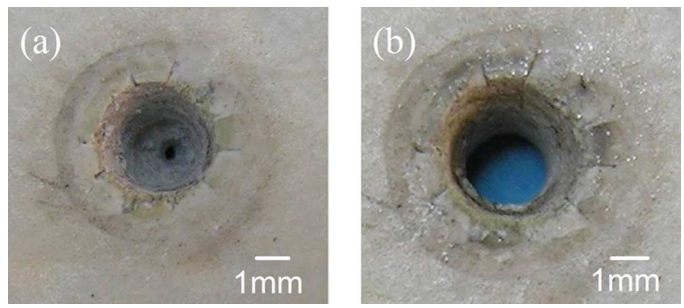

Fig. 14. Stepwise mechanically assisted microwave drilling of a 7-mm-thick ceramic tile. (a) Initial dimple after a slight mechanical removal of the porous region caused by the localized microwaves. (b) Final hole obtained after four repetitive steps.

porous debris by a slight manual grinding. This results for instance in the ∼ 3-mm$^{\emptyset}$ opening in the glass plate shown in Fig. 13. The removal of the soft porous debris is performed, for instance, by a slowly rotating reamer, either separated or integrated as a hollow reamer on the outer cylinder of the coaxial structure [2].

An intentional stepwise mechanically assisted drilling procedure was examined also on 7-mm-thick ceramic tiles (EURO collection EN14411). Through holes were drilled by applying a 100-W incident power to a 1-mm$^{\emptyset}$ drill-bit in four repeating steps, as shown in Fig. 14(a) and (b). Each step includes the insertion of the drill bit into the substrate after the hotspot has formed (in a ∼ 10-s TTM) and then a slight mechanical grinding to remove the debris. The stepwise drilling process helps to avoid damages to the bulk that could happen during continuous drilling due to thermal and mechanical stresses [though it does not prevent some imperfections as seen in Fig. 14(b)].

The center electrode might be coated slightly by a glossy layer during the microwave-drill operation in materials such as silicates and ceramics. This fragile thin coat can be removed easily to renew the electrode. The optional plasma mode [as in Fig. 11(a)] may erode the electrode, hence it may need a replacement after approximately five to ten operations in this mode.

Apart from drilling, the localized heating capabilities of the solid-state microwave-drill device may lead to a wide variety of applications and processes in different materials. Fig. 15(a) shows for instance melting and nailing of basalt by ∼ 100-W microwave power using a 1-mm$^{\emptyset}$ drill bit. Fig. 15(b) shows indentation of basalt by moving the microwave drill bit over its surface in the required pattern (the letter **A**, in this case).

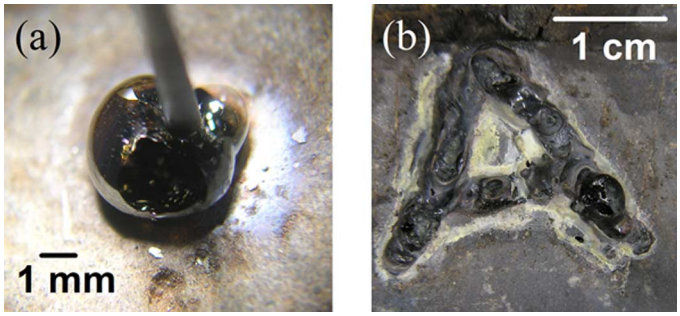

Fig. 15. Basalt processing by localized 100-W microwaves. (a) Melting and nail insertion. (b) Surface indentation (the letter A) by successive runs.

V. Discussion

The theoretical and experimental results presented in this paper demonstrate the applicability of relatively low-power microwaves, in the range of 10–100 W available by solid-state devices at the S-band, for localized heating and melting of materials like glass, ceramics, and basalts. A variety of new drilling experiments confirms the low-power microwave-drill feasibility, in agreement with the theoretical results. The microwave *drillability* factor (4), introduced to enable simple estimates, is confirmed by the theoretical model.

The low-power microwave capabilities are demonstrated by a miniature microwave-drill device using an LDMOS-FET amplifier, imported from a cellular base-station application. The localized microwave-material interaction results in a hotspot evolved by self-focused thermal-runaway instability. This effect is characterized by rapid temperature rise accompanied by a steep increase in the microwave absorption, similarly to higher power drills and volumetric thermal-runaway instabilities. The microwave-drill operation in much lower input power than presented before [1]–[3] is enabled by optimizing the inner electrode geometry. The sharpened tip and the narrower diameter increase the concentration of the induced electric field (Fig. 3), and enable the intentional thermal-runaway effect in lower power, down to $\sim$ 10 W as well. This power reduction enables compact solid-state implementations and eases the technology proliferation for delicate applications (e.g., bone drilling in orthopedic operations [11] and various processes in the electronics industry [9], [13], [14]).

The effectiveness of the low-power localized microwave interaction could be improved significantly by an adaptive impedance matching of the dynamically varying medium. The load impedance varies during the interaction from an open circuit to much lower impedance, within seconds. In the experiments presented here, the initial effective power was a relatively small portion ($< 20\%$) of the total microwave power, and it increased with the hotspot formation (e.g., in Fig. 8). An adaptive impedance-matching system, as used in high-power heating systems [38], could either reduce the total power required to reach the same performance, or accelerate the heating process with the given power.

Further improvement of the localized heating process could be achieved by localized plasma preheating as demonstrated in Fig. 11. The initial plasma stage extends the microwave-drill abilities further to hard-start materials, such as pure alumina and various metals [4]. It can be used also as a combustion igniter, e.g., for thermite reactions [39].

The microwave drilling operation also involves the mechanical function of the electrode as a means to penetrate into the hotspot and to deepen the hole. As with the larger microwave drills [2], [5], the miniature ones can be equipped with integrated mechanical elements (e.g., a rotating hollow reamer integrated with the outer coaxial conductor) to extend the microwave drilling and cutting capabilities.

The feasibility of localized microwave heating to above 1000 °C by low-voltage ($\sim$ 30 V) all-solid-state devices opens possibilities for a variety of applications. To some extent, the compact localized microwave heater may provide a low-cost substitute for laser heating applications. One example, in addition to drilling, is the laser-induced breakdown spectroscopy technique for material identification. This can be applied as well by a localized microwave applicator instead of the laser [40]. Further technological developments expected in solid-state high-power microwave sources, including GaN and SiC technologies, and a better scientific understanding of localized microwave heating mechanisms, will lead essentially to a wide range of material-processing applications utilized by low-power localized microwaves.

Acknowledgment

The authors would like to thank O. Aktushev and G. Dvoretzki for their contributions.

References

[1] E. Jerby, V. Dikhtyar, O. Aktushev, and U. Grosglick, "The microwave drill," *Science*, vol. 298, pp. 587–589, 2002.

[2] E. Jerby and V. Dikhtyar, "Method and Device for Drilling, Cutting, Nailing and Joining Solid Non-Conducting Materials using Microwave Radiation," U.S. Patent 6114676, Sep. 5, 2000.

[3] E. Jerby, O. Aktushev, and V. Dikhtyar, "Theoretical analysis of the microwave-drill near-field localized heating effect," *J. Appl. Phys.*, vol. 97, 2005, Art. ID 034909.

[4] E. Jerby, A. Golts, Y. Shamir, S. Wonde, J. B. A. Mitchell, J. L. LeGarrec, T. Narayanan, M. Sztucki, D. Ashkenazi, and Z. Barkay, "Nanoparticle plasma ejected directly from solid copper by localized microwaves," *Appl. Phys. Lett.*, vol. 95, 2009, Art. ID 191501.

[5] E. Jerby and V. Dikhtyar, "Drilling into hard non-conductive materials by localized microwave radiation," in *Proc. 8th Int. Conf. Microw. High-Frequency Heating*, Bayreuth, Germany, Sep. 4–7, 2001, pp. 687–694.

[6] E. Jerby, O. Aktushev, V. Dikhtyar, P. Livshits, A. Anaton, T. Yacoby, A. Flax, A. Inberg, and D. Armoni, "Microwave drill applications for concrete, glass and silicon," in *Proc. 4th World Congress Microw. Radio-Frequency Applications*, Austin, TX, Nov. 4–7, 2004, pp. 156–165.

[7] S. R. Wylie, A. I. Al-Shamma'a, and A. Shaw, "A microwave plasma drill," in *Proc. IET Conf. High Power RF Tech.*, London, U.K., 2009, pp. 1–3.

[8] E. Jerby, V. Dikhtyar, and O. Aktushev, "Microwave drill for ceramics," *Amer. Ceramic Soc. Bull.*, vol. 82, pp. 35–37, 2003.

[9] X. Wang, W. Liu, H. Zhang, S. Liu, and Z. Gan, "Application of microwave drilling to electronic ceramics machining," in *Proc. 7th Int. Conf. Electron. Packaging Technol.*, Shanghai, China, Aug. 26–29, 2006, Art. ID 4198945.

[10] E. Jerby, V. Dikhtyar, and M. Einat, "Microwave melting and drilling of basalts," in *Proc. AIChE Annu. Meeting*, Austin, TX, Nov. 4–7, 2004, p. 1673.

[11] Y. Eshet, R. Mann, A. Anaton, T. Yacoby, A. Gefen, and E. Jerby, "Microwave drilling of bones," *IEEE Trans. Biomed. Eng.*, vol. 53, no. 6, pp. 1174–1182, Jun. 2006.

[12] E. Jerby and A. M. Thompson, "Microwave drilling of ceramic thermal barrier coatings," *J. Amer. Ceram. Soc.*, vol. 87, pp. 308–310, 2004.

[13] R. Herskowits, P. Livshits, S. Stepanov, O. Aktushev, S. Ruschin, and E. Jerby, "Silicon heating by a microwave-drill applicator with optical interferometric thermometry," *Semicond. Sci. Technol.*, vol. 22, pp. 863–869, 2007.
[14] P. Livshits, V. Dikhtyar, A. Inberg, A. Shahadi, and E. Jerby, "Local doping of silicon by a point-contact microwave applicator," *Microelectron. Eng.*, vol. 88, pp. 2831–2836, 2011.
[15] F. Marken, Y. C. Tsai, B. A. Coles, S. L. Matthews, and R. G. Compton, "Microwave activation of electrochemical processes: Convection, thermal gradients and hot spot formation at the electrode solution interface," *New J. Chem.*, vol. 24, pp. 653–658, 2000.
[16] L. J. Cutress, F. Marken, and R. G. Compton, "Microwave-assisted electroanalysis: A review," *Electroanalysis*, vol. 21, pp. 113–123, 2009.
[17] I. Longo and A. S. Ricci, "Chemical activation using an open-end coaxial applicator," *J. Microw. Power Electromagn. Energy*, vol. 41, pp. 1–4, 2007.
[18] G. B. Gentili, M. Linari, I. Longo, and A. S. Ricci, "A coaxial microwave applicator for direct heating of liquids filling chemical reactors," *IEEE Trans. Microw. Theory Tech.*, vol. 57, no. 9, pp. 2268–2275, Sep. 2009.
[19] T. Z. Wong and B. S. Trembly, "A theoretical model for input impedance of interstitial microwave antennas with choke," *Int. J. Rad. Oncol. Biol. Phys.*., vol. 28, pp. 673–682, 1994.
[20] I. Longo, G. B. Gentili, M. Cerretelli, and N. Tosoratti, "A coaxial antenna with miniaturized choke for minimally invasive interstitial heating," *IEEE Trans. Biomed. Eng.*, vol. 50, no. 1, pp. 82–88, Jan. 2003.
[21] A. Copty, F. Sakran, M. Golosovsky, and D. Davidov, "Low-power near-field microwave applicator for localized heating of soft matter," *Appl. Phys. Lett.*, vol. 24, pp. 5109–5111, 2004.
[22] C. L. Brace, "Microwave ablation technology: What every user should know," *Curr. Problem Diagnst. Radiol.*, vol. 38, pp. 61–67, 2009.
[23] W. A. G. Voss, "Solid-state microwave oven development," *J. Microw. Power*, vol. 21, pp. 188–189, 1986.
[24] E. Schwartz, A. Anaton, D. Huppert, and E. Jerby, "Transistor-based miniature microwave heater," in *Proc. IMPI 40th Annu. Int. Microw. Symp.*, Boston, MA, 2006, pp. 246–249.
[25] O. Hammi and F. M. Ghannouchi, "Comparative study of recent advances in power amplification devices and circuits for wireless communication infrastructure," in *Proc. 16th IEEE Int. Conf. Electron., Circuits, Syst.*, Tunisia, 2009, pp. 379–382.
[26] H. Blanck, J. R. Thorpe, R. Behtash, J. Splettstößer, P. Brückner, S. Heckmann, H. Jung, K. Riepe, F. Bourgeois, M. Hosch, D. Köhn, H. Stieglauer, D. Floriot, B. Lambert, L. Favede, Z. Ouarch, and M. Camiade, "Industrial GaN FET technology," *Int. J. Microw. Wireless Technol.*, vol. 2, pp. 21–32, 2010.
[27] G. Chen, Z. Chen, S. Hai, P. Wu, Z. Li, and Z. Feng, "Microwave power of S-band 20 mm SiC MESFETs," in *Proc. IEEE Int. Conf. Electron Devices Solid-State Circuits*, 2009, pp. 484–486.
[28] O. Latry, P. Dherbécourta, K. Mourguesa, H. Maananeb, J. P. Sipmab, F. Cornub, P. Eudelineb, and M. Masmoudic, "A 5000 h RF life test on 330-W RF-LDMOS transistors for radars applications," *Microelectron. Reliabil.*, vol. 50, pp. 1574–1576, 2010.
[29] O. Mela and E. Jerby, "Miniature transistor-based microwave drill," in *Proc. Global Congress Microw. Energy Applications*, Otsu, Japan, 2008, pp. 443–446.
[30] Y. Meir, A. Salzberg, and E. Jerby, "Hotspot induced by low-power microwave drill – Transistor-based localized heaters and their new applications," in *Proc. Ampere 13th Int. Conf.*, Toulouse, France, Sep. 5–8, 2011, pp. 201–204.
[31] Y. Alpert and E. Jerby, "Coupled thermal-electromagnetic model for microwave heating of temperature-dependent dielectric media," *IEEE Trans. Plasma Science*, vol. 27, no. 2, pp. 555–562, Apr. 1999.
[32] K. G. Ayappa, H. T. Davis, E. A. Davis, and J. Gordon, "Analysis of microwave heating of materials with temperature-dependent properties," *AIChE J.*, vol. 37, pp. 313–322, 2004.
[33] B. G. McConnell, "A coupled heat transfer and electromagnetic model for simulating microwave heating of thin dielectric materials in a resonant cavity," M.Sc. thesis, Dept. Mech. Eng., Virginia Poly. Inst., Blacksburg, VA, 1999.
[34] U. Kolberg and H. Roemer, "Microwave heating of glass," in *Microwave: Theory and Application in Materials Processing V*, D. E. Clark, J. G. P. Binner, and D. A. Lewis, Eds. Westerville, OH: Amer. Ceram. Soc., 2000, vol. 3, Ceramic Transactions, pp. 527–533.
[35] G. A. Kriegsmann, "Thermal runaway in microwave heated ceramics: A 1-D model," *J. Appl. Phys.*, vol. 71, pp. 1960–1966, 1992.
[36] X. Wu, J. R. Thomas, and W. A. Davis, "Control of thermal runaway in microwave resonant cavities," *J. Appl. Phys.*, vol. 92, pp. 3374–3380, 2002.
[37] G. A. Kriegsmann, "Hot spot formation in microwave heated ceramic fibers," *IMA J. Appl. Math.*, vol. 59, pp. 123–148, 1997.
[38] V. Bilik and J. Bezek, "Automatic impedance matching under high power complex signal conditions," in *Proc. IEEE 19th Int. Conf. Radioelektronika*, Bratislava, Slovakia, Apr. 22–23, 2009, pp. 141–144.
[39] Y. Meir and E. Jerby, "Thermite-powder ignition by electrically-coupled localized microwaves," *Combust. Flames*, vol. 159, pp. 2474–2479, 2012.
[40] Y. Meir and E. Jerby, "Breakdown spectroscopy induced by localized microwaves for material identification," *Microw. Opt. Technol. Lett.*, vol. 53, pp. 2281–2283, 2011.

Yehuda Meir (S'11) was born in Bat-Yam, Israel, in 1983. He received the B.Sc. and M.Sc. (*cum laude*) degrees in electrical electronic engineering from Tel Aviv University, Tel Aviv, Israel, in 2010 and 2011, respectively, where he is currently working toward the Ph.D. degree under the supervision of Prof. Eli Jerby at the Department of Physical Electronics.

His current research interests include microwave localization, microwave-drill technology, thermite ignition, fireballs, and plasmoids in both scientific and technological aspects.

Mr. Meir received the Best Poster Award at the 13th AMPERE International Conference on Microwave and High Frequency Heating, Toulouse, France, September 2011, for his study on rapid heating by localized microwaves. He was awarded the Colton Scholarship in 2012.

Eli Jerby (M'11) received the Ph.D. degree in electrical engineering from Tel Aviv University, Tel Aviv, Israel, in 1989.

He was a Rothschild and Fulbright Post-Doctoral Fellow with the Research Laboratory of Electronics, Massachusetts Institute of Technology. Since his return to Tel Aviv University, Tel Aviv, Israel, in 1991, he has studied novel schemes of microwave radiation sources, microwave localization effects and their applications (e.g., microwave-drill invention), microwave-induced plasmas, plasmoids, and fireballs. He is currently a Professor with the Faculty of Engineering, Tel Aviv University.